Biointerface Research in Applied Chemistry
Open-Access Journal (ISSN: 2069-5837)

*Article*
**Volume 13, Issue 5, 2023, 453**
https://doi.org/10.33263/BRIAC135.453

# Hirshfeld Surfaces Analysis and Computational Approach of Hybrid Organic-Inorganic Phosphate

**Abdellatif Rafik [1,*], Hafid Zouihri [2], Taoufiq Guedira [1]**

[1] Laboratory of Organic Chemistry, Catalysis and Environment Laboratory, Faculty of Sciences, Ibn Tofail University, B.P. 133, 14000 Kenitra, Morocco
[2] Laboratory of Materials Chemistry and Biotechnology of Natural Products, Moulay Ismail University, Faculty of Sciences, Meknes city, Morocco
* Correspondence:rafik2013abdellatif@gmail.com (A.R);

Scopus Author ID 57222128782
**Received: 2.04.2022; Accepted: 5.06.2022; Published: 21.12.2022**

**Abstract:** The present work focuses on the Anilinium dihydrogen phosphate [ADHP]. Quantum chemistry and Hirshfeld surface analyses are used in the study.This work was carried out to investigate and quantify the contributions and the various intermolecular interactions within crystals. This analysis reveals that O…H and H…H, the intermolecular interactions in the compound, were studied using Hirshfeld surface analysis. These results show that both compounds exhibit similar features, however, the energy gap between $E_{HOMO}$ and $E_{LUMO}$ obtained from the molecular orbital analysis indicates that compound ADHP is analyzed by a molecular structural more favorable for charge transfer, The Mulliken Atomic Charges and Density of state (DOS).

**Keywords**: DOS; Homo-Lumo; intermolecular interactions; Hirshfeld surface analysis.



## 1. Introduction

Recently, organic-phosphates have been intensively studied due to their many uses in various fields such as biomolecular sciences, catalysts, and nonlinear optics [1]. Among Particularly important are the hybrid compounds investigated, organic phosphates formed as a result of the inorganic oxy-acid reaction such as orthophosphoric acid ($H_3PO_4$) and organic amines. Organic monohydrogen ($HPO_4^{2-}$) and dihydrogen phosphate ($H_2PO_4$-) compounds provide a class of materials with numerous practical and potential uses in various fields such as biomolecular sciences, catalysis, and liquid crystal-material development, ferroelectrics, nonlinear optical and supramolecular studies [2, 4].

Organic and inorganic hybrid research based on acid-mediated interactions showing strong optical nonlinearity, mechanical strength, and thermal stability [5] suggests that highly polarizable cations responsible for the NLO properties in these systems are combined with inorganic anions by intermolecular hydrogen bonding that creates a crystal structure non-centrosymmetric. Bifurcated Hydrogen bonds have been shown to be responsible for the structural stability of supramolecular structures [6, 7], and the transfer of charges from the organic part to the inorganic part results in a strong nonlinear response [8]. The hydrogen bond network in a single molecule leads to its high values of hyperpolarizability and charging interactions, making it useful in nonlinear optical applications such as frequency conversion, optical modulation, Hirshfeld surface analysis, and optical switching [9–11].

This work reports the theoretical geometry was calculated using the Hirshfeld surface analysis of the ADHP compound. Computationally, the molecular electrostatic potential (MEP), frontier orbitals (HOMO-LUMO), the density of state (DOS), and Mulliken population analysis were derived. The acronym B3LYP and HF methods with basis set 3-21G were for the theoretical calculations.

## 2. Materials and Methods

### *2.1. Experimental*

Aniline (99.8%, Sigma-Aldrich) was purified via the preparation of anilinium chloride. Raw aniline was mixed with 2 M HCl with cooling, and the solution was filtered through active carbon. The filtrate was concentrated in vacuo, and crystallization of anilinium chloride was carried out in a refrigerator. After filtration, the solution was evaporated in a vacuo, providing purified aniline. This was mixed with 0.03 M $H_3PO_4$ (Sigma-Aldrich, pure 85%), the concentration of which was determined by titration on methyl orange in a 1:1.5 molar ratio. The resulting mixture was stirred with heating at 313 K and further diluted in order to dissolve the small amount of salts formed immediately upon mixing. Finally, the solution was filtered, and the filtrate was left to crystallize very slowly in the air at room temperature.

### *2.2. Quantum chemical computations.*

DFT and HF calculations were achieved using Gaussian 03 package [12]. The equilibrium structures were fully relaxed and optimized using DFT/B3LYP and HF [13, 14] approach and 3-21G basis sets. The HOMO-LUMO band gaps were calculated as a difference between the lowest empty molecular orbitals and highest occupied molecular orbitals (HOMO) orbitals (LUMO) energies, Density of state (DOS), and Mulliken. The studied structures were visualized, and electron density was assigned using Gauss view [15] programs.

### *2.3. Hirshfeld surface analysis*

An effective method for calculating the intermolecular interactions of molecular crystals is Hirshfeld surface analysis. Crystal Explorer 3.1 was used to create the Hirshfeld surfaces [16], and fingerprint plots [17] were exhibited here. The normalized contact distance (dnorm) was determined using the following expression: $d_e$ (distance from a point on the surface to the nearest nucleus outside the surface) $d_i$ (distance from a point on the surface to the nearest nucleus within the surface):

$$\mathbf{d}_{\mathbf{norm}} = \frac{(\mathbf{d}_{\mathbf{i}} - \mathbf{r}_{\mathbf{i}}^{\mathbf{vdw}})}{\mathbf{r}_{\mathbf{i}}^{\mathbf{vdw}}} + \frac{(\mathbf{d}_{\mathbf{e}} - \mathbf{r}_{\mathbf{e}}^{\mathbf{vdw}})}{\mathbf{r}_{\mathbf{e}}^{\mathbf{vdw}}}$$

where $r_i^{vdW}$ is the atom's van der Waals radius inside the surface. Hirshfeld and $r_e^{vdW}$ is the atom's van der Waals radius outside the surface Hirshfeld. The title compound Hirshfeld surface uses a color gradient that ranges from red (distances shorter than vdW with a negative $d_{norm}$ value) to white (represents the touch between blue and around vdW separation with a $d_{norm}$ value of zero (distances longer than vdW with a positive $d_{norm}$ value). The red dots on the surface the Hirshfeld surface show the interconnections in the hydrogen bonds [18, 19]. O-H...O and N-H...O hydrogen-bonding interactions are thought to be the cause of the red circular

collapse. With a standard (high) surface resolution, the surfaces of 3D dnorm are displayed over a set color range of 0.377 (red) to 1.533 (blue)Å.

## 3. Results and Discussion

### *3.1. Crystal structure.*

Detailed crystal structure data is the asymmetric unit in single crystals of ADHP containing one independent molecule of triclinic system with *P-1* space group. The plot of ORTEP and the optimized ADHP In Figure 1, the molecular structure is displayed. The overall view of the title compound packaging is shown in Figure 2. The lattice and unit cell parameters are *a*= 8.8040 (3) Å, *b*= 10.4220 (4) Å, *c*= 14.0890 (6) Å, α= 86.418 (2), and β= 75.8890 (19) °. In this crystal structure, the existence of the hydrogen phosphate anion is verified by the P — O bond distances, and the presence of a related density peak at a distance from the oxygen atom $O_1$ confirms the anion hydroxyl group. The bond distance [$P_1$—$O_1$ = 1.559 (2) Å] indicates a single-bond character, while the bond distances [$P_1$—$O_2$ = 1.563 (2), $P_1$— $O_3$ = 1.497(2) and $P_1$—$O_4$ = 1.513 (2) Å] reveal the resonating P—O bonds of the hydrogen phosphate anion. As expected, in both cations, the C— N bond [$C_{11}$—$N_{11}$ = 1.471 (3), $C_{31}$—$N_{31}$ = 1.473 (3) Å] involving the ammonium group is longer than that in the amine group [$C_{21}$—$N_{21}$ = 1.467 (3) Å]. The phenyl rings of the anilinium cations are almost perpendicular to one another; in line with the individual N…O separations, these hydrogen bonds formally belong to three groups: firstly, three rather short and thus strong hydrogen bonds with N…O separations in the range 2.743 (3)–2.791 (2) Å, secondly, five medium-strong hydrogen bonds lying in the range 2.818 (2)– 2.924 (2) Å, and finally, four weaker hydrogen bonds with the largest N…O separations, viz. 2.965 (2) –3.296 (2) Å. Considering the unimodal distribution of well-defined N…O contact distances, the N…O distances of the first and third groups are among those found less frequently, being either significantly shorter or longer than the mean value.

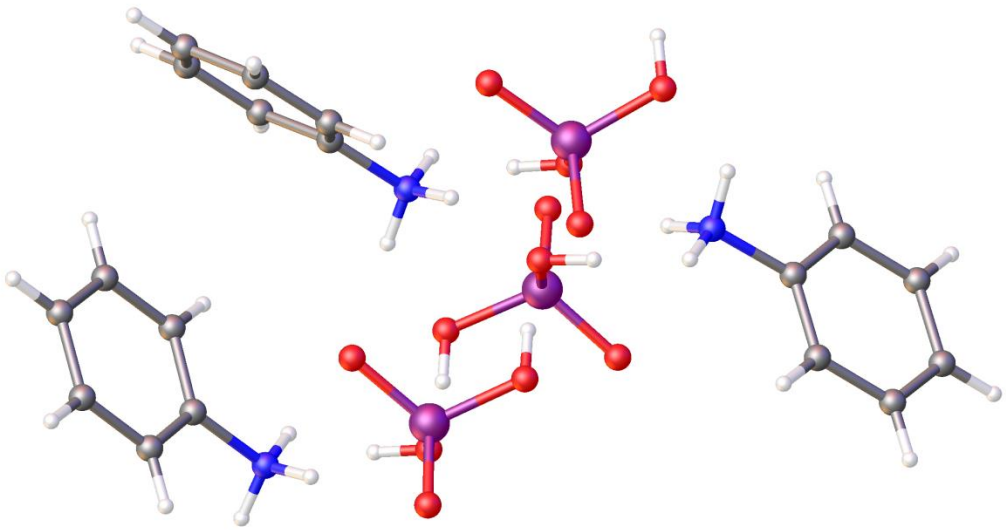

**Figure 1**. A view of the atom labels on the ADHP compound's molecular structure. Drawn are displacement ellipsoids to a probability 50% level.

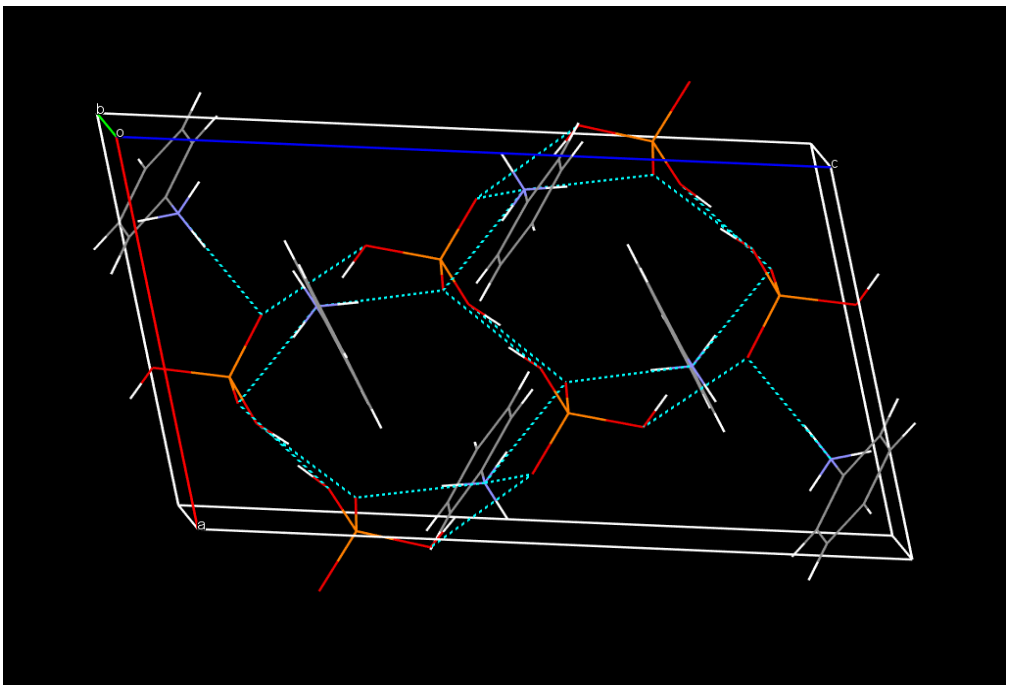


**Figure 2**. Normal view to the plane (101) of the title compound's crystal packing, the N—H … O hydrogen bonds are represented by dashed lines.

*3.2. Hirshfeld surface analysis.*

The intermolecular interactions in crystal packing of ADHP have been analyzed using Hirshfeld surface (HS) and their corresponding two-dimensional fingerprint plots. Hirshfeld surface analysis is a graphical tool used to study the hydrogen bonds, intermolecular interactions, and their significance for crystal packing stability. Hirshfeld surface is mapped using $d_{norm}$ descriptor when it encompasses two factors, namely $d_e$ and $d_i$. $d_e$ represents the distance between the surface point and nearest interior atoms, and di represents the distance between the surface point and nearest exterior atoms [20]. The two-dimensional $d_e/d_i$ fingerprint plots exhibit significant differences from the interactions [21] occurring in the crystal packing of the ADHP molecule. To provide context, the overall fingerprint pattern in the outline of ADHP is shown in the grey background, and the blue dotted area shows the separate contact. The $d_{norm}$ and 2D-fingerprint plot (100% interactions) of ADHP is shown in Figure 3. Red-blue-white color scheme mapped in Hirshfeld surface using $d_{norm}$ descriptor. White and the Van der Waals radii are equal, while the Van der Waals radii of red and blue are different. The red regions in Figure 3 visualize the H…H, O…H, H…C and C…C intermolecular contacts, respectively. The various fingerprint plots of ADHP have shown in Figure 4, the decomposing fingerprint plot of ADHP in the crystal lattice, highlighting separately the H···O (41.0%), H···H (38.2%), H···C/C···H (17.9%), C···C (2.6%), O···O (0.3%), intermolecular contacts. The $d_e$, $d_i$, shape index, and curvedness surfaces of ADHP are shown in Figure 3. The various intermolecular contacts are verified using $d_e$ and $d_i$ surfaces.

To distinguish the ADHP solvent molecule donor and acceptor groups involved in hydrogen bonding, the HS mapped over the electrostatic potential was determined using TONTO with standard STP-3 G base settings set at Hartree – Fock theory. The appearance of blue and red surface regions indicates the positive and negative electrostatic potential, as shown in Figure 5, suggesting that the carbonyl oxygen atom of the amide group and the non-protonated oxygen atom of the carboxylate group act as hydrogen-bond acceptors, whereas the nitrogen/ hydrogen atoms of the amino group and the protonated oxygen atom of the carboxy

group as well as the carbon/ hydrogen atoms of the aromatic moiety act as hydrogen-bond donors [22, 23].

The planar stacking arrangement of C···C is identified by closer red and blue triangles from the shape index. The molecules bearing aromatic rings are involved in π···π contacts, which are confirmed by the presence of flat green surface areas of C···C contribution to curvedness surface (Figure 3(e)). The 2.6 % contribution of C···C from the fingerprint plot represents the π-stacking interactions in ADHP. A quite high contribution of H···H contacts to the Hirshfeld surface is shown by aromatic moiety-bearing organic molecular crystals. From the result, it emerges that the intermolecular interaction H···H shows a major contribution of 38.2% from the Hirshfeld surface, shown in Figure 6.

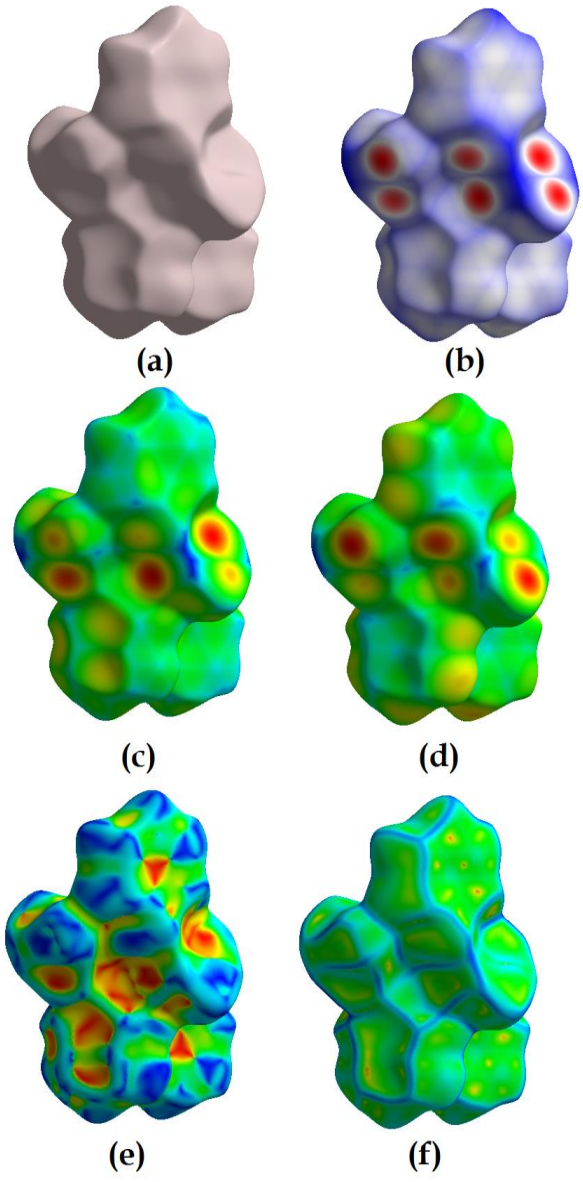


**Figure 3.** Hirshfeld surface mapped with (**a**)None; (**b**) $d_{norm}$; (**c**) $d_i$; (**d**) $d_e$; **(e)** shape index; (**f**) curvedness for the ADHP compound.

The voids in the crystal structure of ADHP. Those are based on calculating the densities of the spherical atomic electron at the correct nuclear location. The measurement of crystal voids (results below 0.002 a.u. isovalue) indicates the vacuum volume of the title compound of 118.98 $Å^3$ and surface area of 403.64 $Å^2$. We note that the isosurfaces with electron density are not fully closed around the components but are open at the locations where interspecies

approaches are found, e.g., N-H…H. By simply generating an isosurface of the procrystal electron density, voids can be observed and investigated. Figure 7 depicts the void surface for ADHP with a volume of 1243.71 $Å^3$ per unit cell and an isosurface of 0.002 a.u. The isovalue 0.002 a.u. covers 99.9% of the electron density region, which is important for delineating molecular voids. It is discovered that voids take up around 9.56% of the volume of a unit cell (Figure 7). The voids in the ADHP crystal structure are displayed in a consistent pattern of parallel layers that are normal to the [100]. The presence of void generates a low packing density [100], which minimizes the likelihood of slipping along it. Furthermore, it concludes that ADHP crystal has a softer nature and a low voids percentage [24].

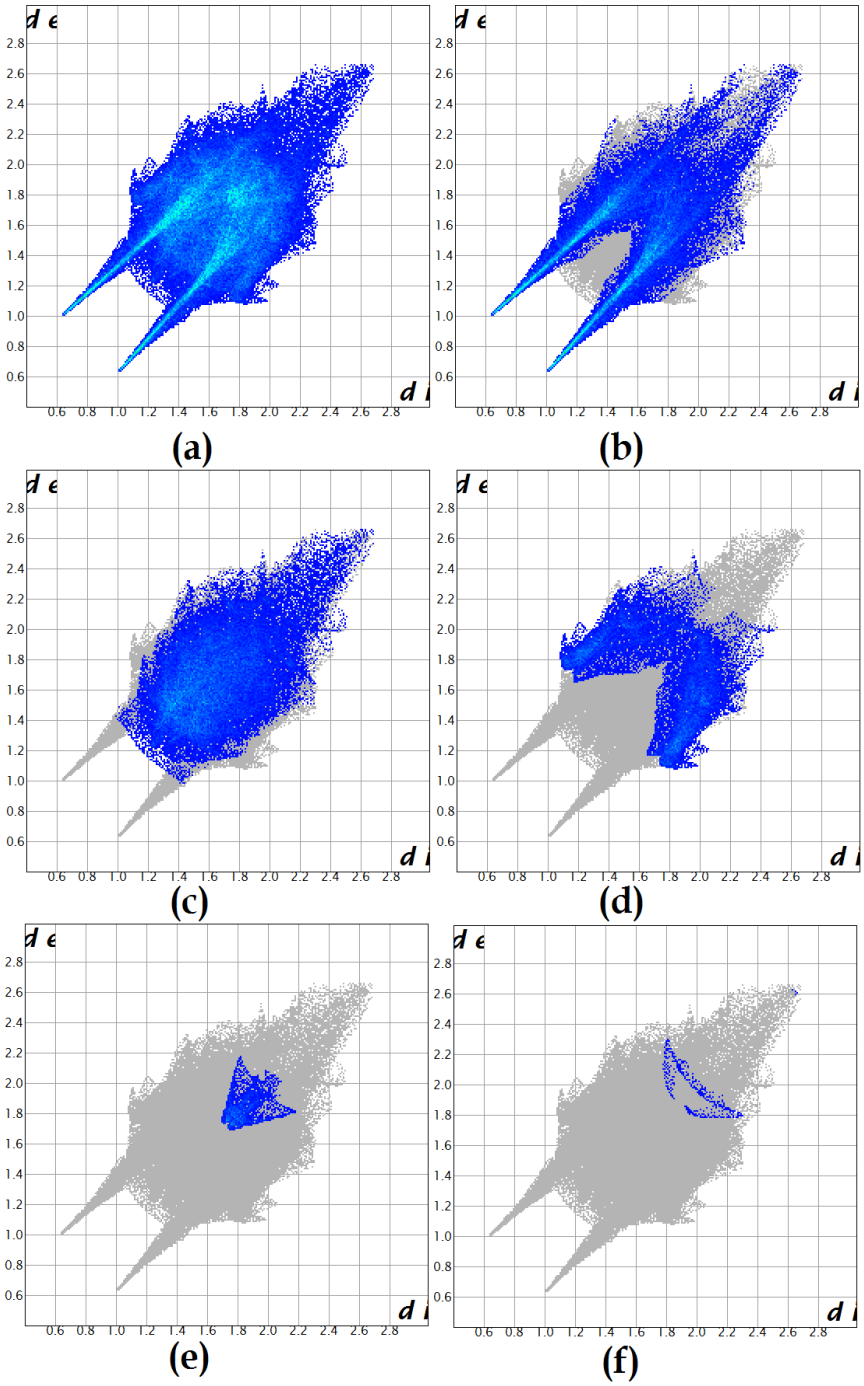


**Figure 4.** The complete fingerprint layouts in two dimensions for the ADHP, showing all interactions: (**a**) all interactions; (**b**) H…O/O…H contacts; (**c**) H…H contacts; (**d**) H…C/C…H contacts; (**e**) C…C contacts; (**f**) O…O contacts.

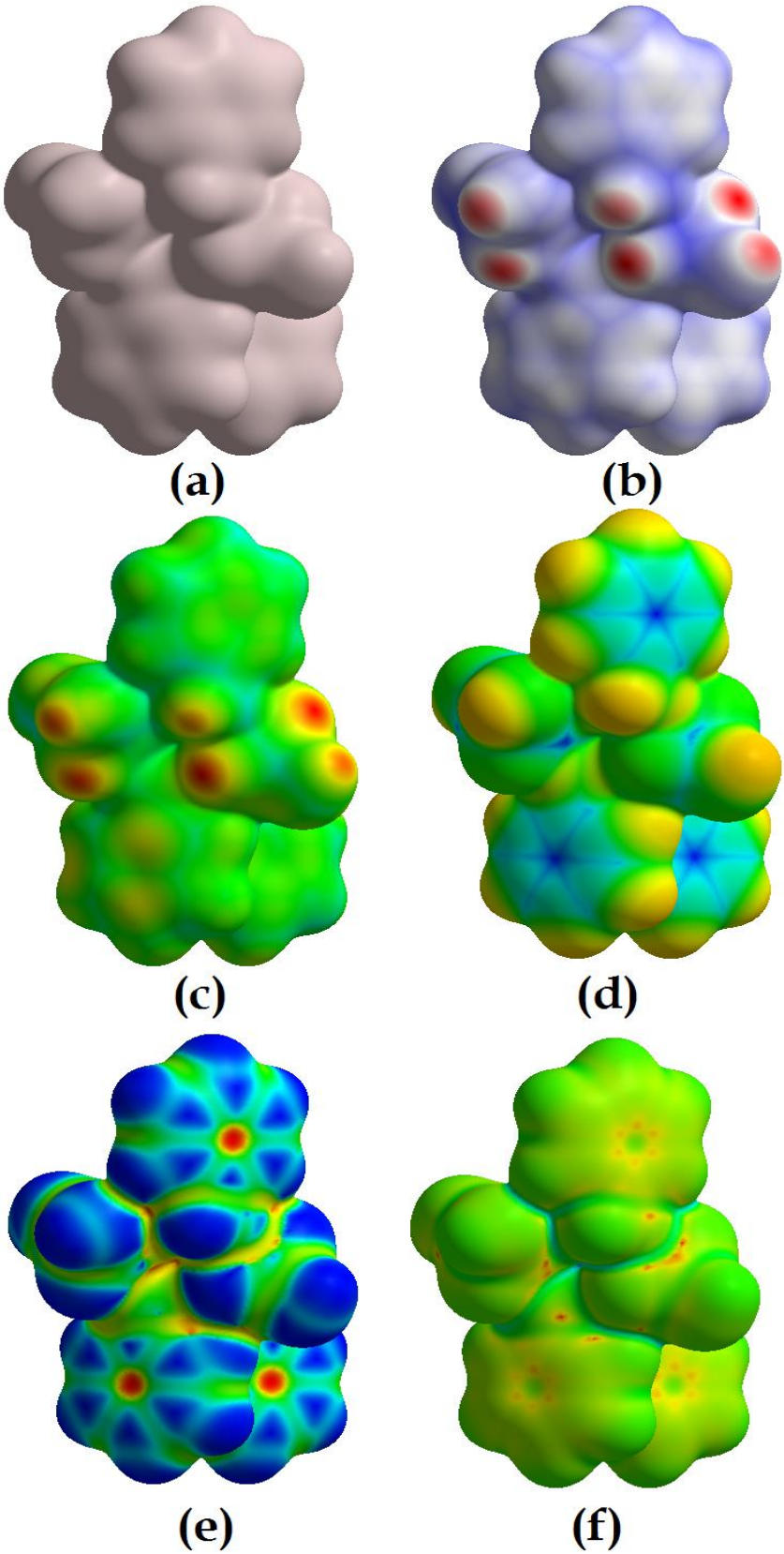


**Figure 5**. Electrostatic Potential (PE) mapped on Hirshfeld surface of the molecule of ADHP: **(a)**None; **(b)** $d_{norm}$; **(c)** $d_e$; **(d)** $d_i$; **(e)** Shape index; **(f)** Curvedness.

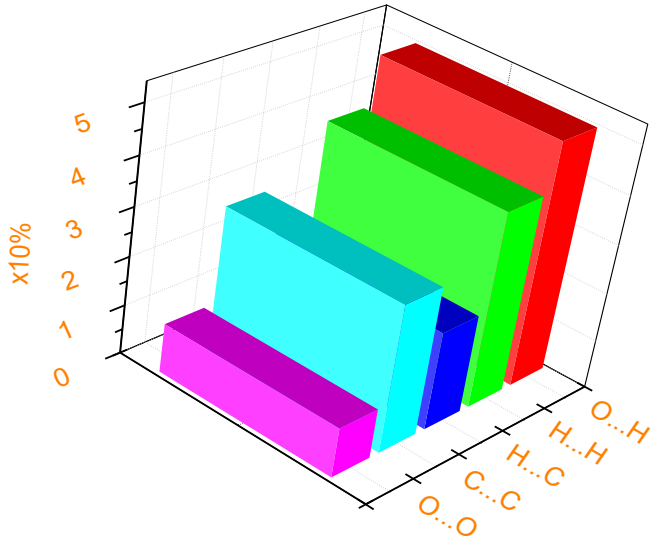


**Figure 6.** Percentage contributions of interatomic contacts to the Hirshfeld surface for the ADHP compound.

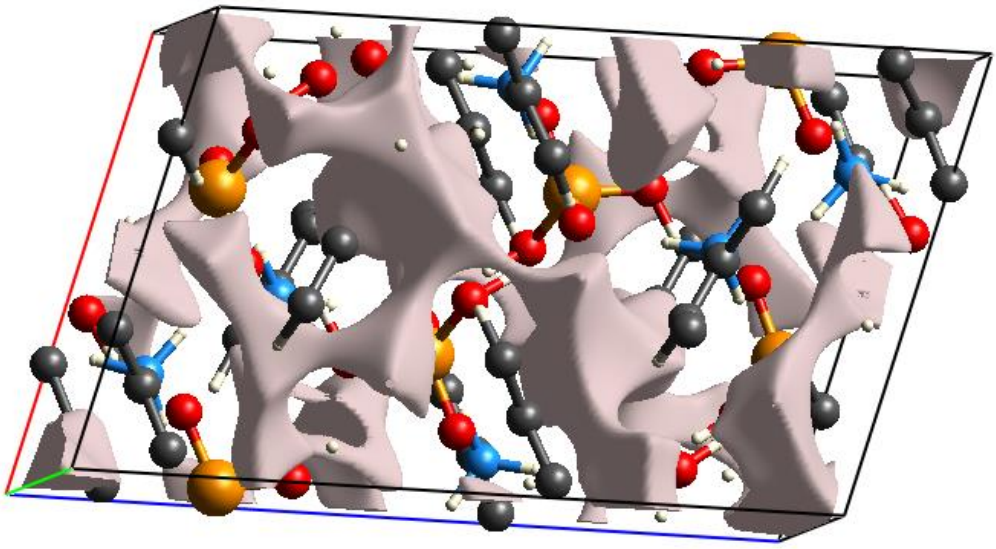

**Figure 7.** Crystal Voids of ADHP isosurface at 0.002 a.u. The volume occupied by voids is approximately 9.56% of the volume of the unit cell.

*3.3. Geometry optimization.*

The optimized structure parameters of ADHP calculated by DFT, B3LYP level, and HF methods with the 3-21G basis set are listed in Table 1; the atom numbering scheme is given in Figure 8. Experimental values of bond lengths and angles of ADHP conformer is given in Table 1. For example, the optimized bond lengths of (C-C) in falls in the range [1.3768 -1.3904 Å] for B3LYP method are in good agreement with those of experimental bond lengths; the optimized bond length of (C-N) in falls in the range [1.4673- 1.4734 Å] They exhibit strong concordance with those found in experimental x-ray data. The optimized bond lengths of (P-O) adjacent ring by HF & DFT are found to be in the range [1.5006 - 1.5622 Å], which are also in good agreement with experimental values that fall in the range [1.497-1.563 Å]. For the studied molecule, the dipole moments were calculated by DFT as 2.4080 Debye and HF as 1.0978 Debye.

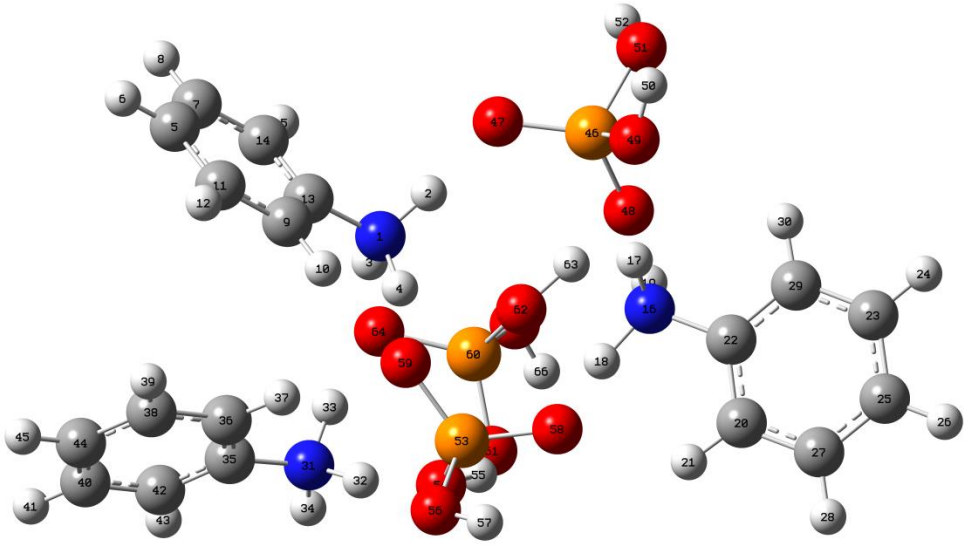

**Figure 8**. Optimized geometry of the title molecule.

**Table 1**. Comparison of experimental and theoretical optimized parameter values of the ADHP [bond length in (Å].

| Parameters | Experimental | DFT/B3LYP/3-21G | HF/3-21G |
|---|---|---|---|
| R(1,2) | 1.0513 | 1.0682 | 1.0806 |
| R(1,3) | 1.0302 | 1.0593 | 1.0802 |
| R(1,4) | 1.0621 | 1.0999 | 1.1147 |
| R(1,13) | 1.4625 | 1.4723 | 1.4732 |
| R(2,47) | 1.6193 | 1.6374 | 1.6291 |
| R(3,64) | 1.8620 | 1.768 | 1.7007 |
| R(4,59) | 1.5535 | 1.5073 | 1.4994 |
| R(5,6) | 1.0718 | 1.0838 | 1.0928 |
| R(5,7) | 1.3844 | 1.3971 | 1.4051 |
| R(5,11) | 1.3842 | 1.3972 | 1.4053 |
| R(7,8) | 1.0716 | 1.0836 | 1.0928 |
| R(7,14) | 1.3836 | 1.3962 | 1.4041 |
| R(9,10) | 1.0711 | 1.0841 | 1.0941 |
| R(9,11) | 1.3840 | 1.3961 | 1.4039 |
| R(9,13) | 1.3822 | 1.3965 | 1.4054 |
| R(11,12) | 1.0719 | 1.0840 | 1.0933 |
| R(13,14) | 1.3806 | 1.3940 | 1.4025 |
| R(14,15) | 1.0716 | 1.0836 | 1.0928 |
| R(16,17) | 1.0156 | 1.0352 | 1.0461 |
| R(16,18) | 1.1107 | 1.1706 | 1.1800 |
| R(16,19) | 1.0358 | 1.0542 | 1.0724 |
| R(16,22) | 1.4677 | 1.4749 | 1.4768 |
| R(18,58) | 1.4067 | 1.3468 | 1.3542 |
| R(19,48) | 1.7264 | 1.7590 | 1.7093 |
| R(20,21) | 1.0701 | 1.0839 | 1.0939 |
| R(20,22) | 1.3801 | 1.3932 | 1.4015 |
| R(20,27) | 1.3845 | 1.3967 | 1.4044 |
| R(22,29) | 1.3816 | 1.3944 | 1.4028 |
| R(23,24) | 1.0714 | 1.0836 | 1.0927 |
| R(23,25) | 1.3853 | 1.3985 | 1.4065 |
| R(23,29) | 1.3829 | 1.395 | 1.4027 |
| R(25,26) | 1.0717 | 1.0837 | 1.0928 |
| R(25,27) | 1.3836 | 1.3972 | 1.4054 |
| R(27,28) | 1.0715 | 1.0836 | 1.0928 |
| R(29,30) | 1.0720 | 1.0841 | 1.0934 |
| R(31,32) | 1.0486 | 1.1276 | 1.1426 |
| R(31,33) | 1.0929 | 1.1051 | 1.1333 |
| R(31,34) | 1.0115 | 1.0285 | 1.0372 |

| Parameters | Experimental | DFT/B3LYP/3-21G | HF/3-21G |
|---|---|---|---|
| R(31,35) | 1.4676 | 1.4715 | 1.4710 |
| R(32,54) | 1.6730 | 1.4605 | 1.4533 |
| R(33,64) | 1.5082 | 1.5385 | 1.4948 |
| R(35,36) | 1.3806 | 1.3949 | 1.4036 |
| R(35,42) | 1.3797 | 1.3940 | 1.4029 |
| R(36,37) | 1.0729 | 1.0874 | 1.0980 |
| R(36,38) | 1.3835 | 1.3957 | 1.4032 |
| R(38,39) | 1.0706 | 1.0829 | 1.0921 |
| R(38,44) | 1.3843 | 1.3970 | 1.4051 |
| R(40,41) | 1.0713 | 1.0835 | 1.0926 |
| R(40,42) | 1.3837 | 1.3960 | 1.4039 |
| R(40,44) | 1.3836 | 1.3965 | 1.4046 |
| R(42,43) | 1.0725 | 1.0848 | 1.0941 |
| R(44,45) | 1.0714 | 1.0835 | 1.0926 |
| R(46,47) | 1.5427 | 1.5668 | 1.5809 |
| R(46,48) | 1.5694 | 1.6109 | 1.6324 |
| R(46,49) | 1.6399 | 1.6892 | 1.7121 |
| R(46,51) | 1.6327 | 1.6741 | 1.6952 |
| R(48,63) | 1.4304 | 1.3292 | 1.3292 |
| R(49,50) | 0.9653 | 0.9936 | 1.0058 |
| R(51,52) | 0.9642 | 0.9925 | 1.0049 |
| R(53,54) | 1.6141 | 1.6402 | 1.6655 |
| R(53,56) | 1.6372 | 1.6815 | 1.7012 |
| R(53,58) | 1.5593 | 1.5962 | 1.6115 |
| R(53,59) | 1.5597 | 1.5952 | 1.6094 |
| R(54,55) | 1.0916 | 1.2921 | 1.2522 |
| R(55,61) | 1.3499 | 1.1629 | 1.2165 |
| R(56,57) | 0.9649 | 0.9955 | 1.0090 |
| R(60,61) | 1.5685 | 1.6204 | 1.6314 |
| R(60,62) | 1.5894 | 1.6148 | 1.6325 |
| R(60,64) | 1.5739 | 1.6026 | 1.6254 |
| R(60,65) | 1.6307 | 1.6704 | 1.6924 |
| R(62,63) | 1.0340 | 1.1139 | 1.1322 |
| R(65,66) | 0.9659 | 0.9962 | 1.0093 |

*3.4. Electrostatic potential (MEP), electron density (ED), and electrostatic potential (EP).*

The calculated electron density cloud covers all atoms in the structure of compound1is illustrated in Figure 9. The electrostatic potential reactivity allows us to find the active sites of ADHP. The oxygen atoms of phosphates molecules anion are sites with the most negative potentials [25-28].

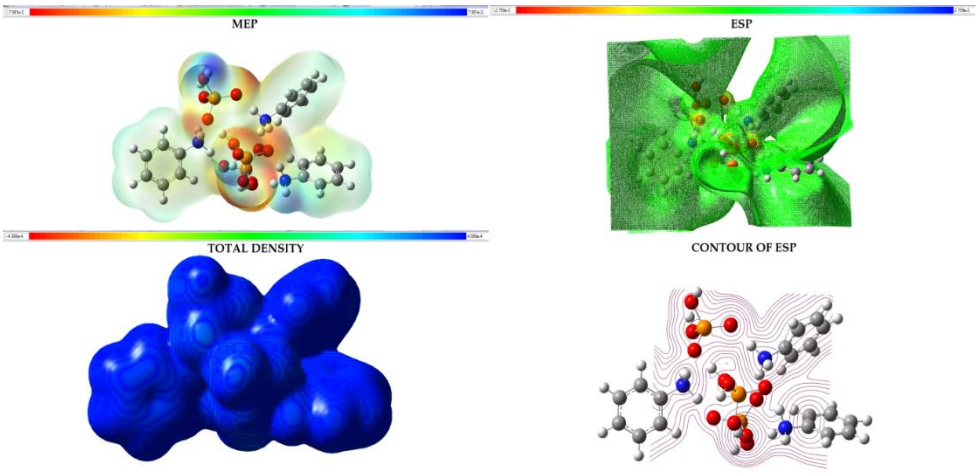


**Figure 9.** The total electron density surface 3D mapped with molecular electrostatic potential (MEP), ED, ESP CONTOUR ESP of ADHP compound.

The Electrostatic Potential Map (EPM) shows negative potentials with red colors, while the blue corresponds to the positive potential areas. The red-brown regions (negative potential) are generally situated over the oxygen atoms. Those regions in this compound are susceptible to a heavy electrophilic attack. The areas with yellow and orange colors, located in the center of the organic molecule, are susceptible to low electrophilic attack. The blue regions around the Anilinium correspond to strong nucleophilic reactivity. Also, Figure 9 shows the total density, contour of total density, alpha density, electrostatic potential, the contour of electrostatic potential, and molecular electrostatic potential.

*3.5. Frontier HOMO-LUMO and Energy gap analysis.*

A good approximation of the reactivity of the molecule could be found by looking at the frontier molecular orbitals (FMO) when frontier molecular orbitals are designated the highest occupied molecular orbitals (HOMO) and the lowest unoccupied molecular orbits (LUMO). HOMO is plausibly known as a contributing electron or nucleophilic, whereas LUMO is an accommodating or electrophilic electron. The energy separation between the HOMO and LUMO determines a molecule's chemical stability and charge molecule-to-molecule transmission [29]. The HOMO-LUMO energy gap is generally the lowest energy electronic excitation possible in a molecule. It is known from Figure 10 that the HOMO is mainly localized on the phosphates of the ADHP molecular system.

In comparison, the LUMO is mainly localized on the title molecule's phenyl ring and $-NH^{3+}$ group. These frontier molecular orbitals indicate the electron density transfer from $C_6H_8N^+$. The red regions represent the positive phases, and the green regions represent the negative phases of ADHP. The energies of HOMO and LUMO are calculated as -0.21559 a.u and -0.06074 a.u, respectively. The energy gap of ADHP is calculated as 4.201 eV.

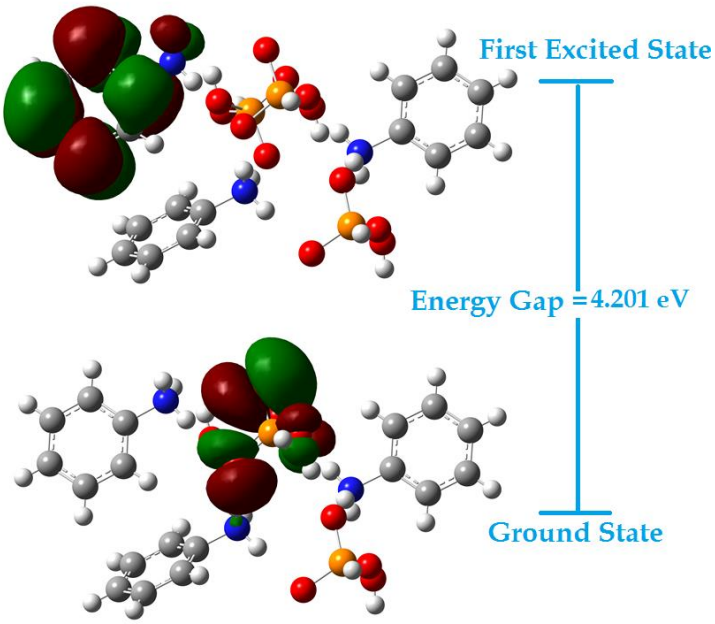


**Figure 10**. Frontier molecular orbital plots of ADHP at the DFT level of theory.

Energies of the FMOs used for the determination of global reactivity descriptors [30], have proposed electrophilicity index as a quantity of energy decreasing as a result of maximum electron transport between donor and acceptor. According to Koopman's theorem, Ionization energy $I = -E_{HOMO}$ and electron affinity $A = -E_{LUMO}$. By using the values of I and A, we can calculate the global reactivity descriptors such as chemical hardness ($\eta = I-A/2$),

electronegativity ($\chi$ = I+A/2), chemical potential ($\mu$ = - (I+A)/2), electrophilicity index ($\omega = \mu^2/2\eta$) and softness (s = 1/$\eta$). The global reactivity descriptors of DTPD are calculated as, Ionization potential I = 0.21559 a.u, electron affinity A = 0.06074 a.u, $\eta$ = 0.0774 a.u, $\chi$ = 0.13816 a.u, $\mu$ = - 0.13816 a.u, $\omega$ = 0.12330 au and s = 12.91572 $a.u^{-1}$, respectively. Based on the narrow energy gap and the chemical hardness ($\eta$) of ADHP, we conclude that this molecule can be classified as a hard molecule.

*3.5. Density of states (DOS).*

The OPDOS charts, often known in the literature as COOP diagrams, are the most crucial tool for illustrating MO compositions and their contributions to chemical bonding. The OPDOS displays if two interacting orbitals, atoms, or groups are bonding, antibonding, or not.An OPDOS positive value indicates a bonding interaction (owing to population positive overlap), a negative value suggests an antibonding interaction (owing to negative population overlap), while a zero value shows no interaction [31, 32]. Furthermore, the OPDOS diagrams enable us to determine and compare ligand donor-acceptor properties and to determine bond and nonbonding properties. The ADHP estimated total electronic state density (DOS) diagrams are shown in Figure. 11. The partial state plot density (PDOS) primarily displays the makeup of the fragment orbitals that contribute to the molecular orbitals depicted in Figure 10.

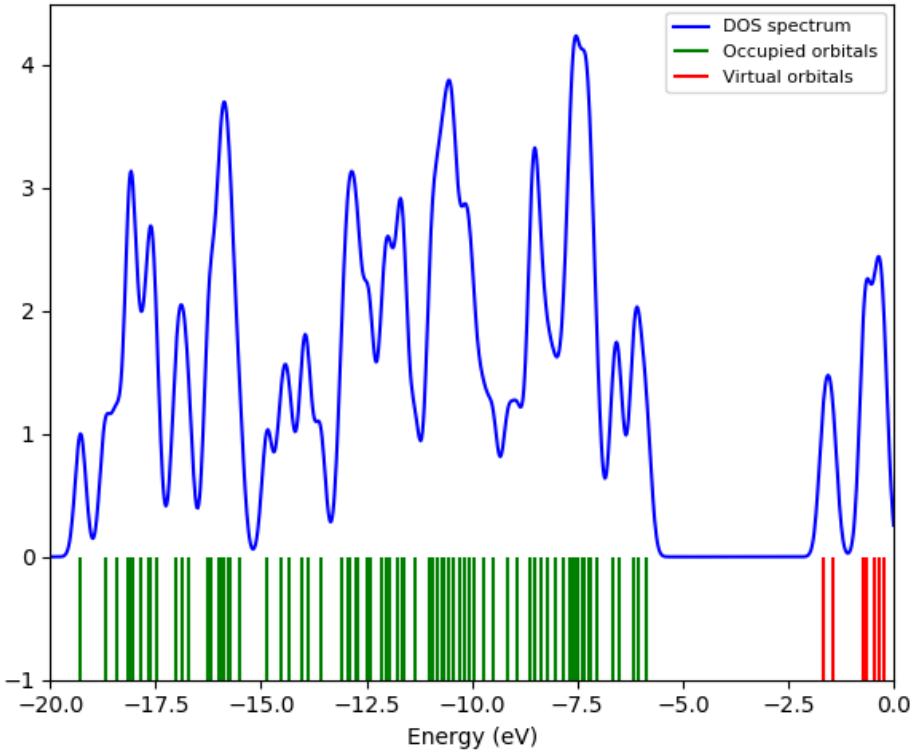


**Figure 11**. The density of state (DOS) spectrum of ADHP compound.

*3.6. Mulliken atomic charges.*

The Mulliken Atomic Charges cannot be experimentally obtained because they do not correspond to physical quantities. Atoms have negatively charged electrons coiled around positively charged nuclei, with no partial charges on the atoms. But the presence of partial charges on the nucleus merely contributes to understanding electron density distribution. The Mulliken population method has been used to obtain complete atomic charge distributions. Mulliken is highly effective in detecting nucleophilic or electrophilic attacks and regions

sensitive to other molecular interactions [33-35]. The molecule study of the Mulliken charging distributions was analyzed using levels 3-21 G of DFT / B3LYP and HF witch. As shown in Figure 12, calculated charges were listed for the title compound. According to Mulliken population analysis results, all hydrogen atoms in the molecule have a positive charge. Mulliken atomic charge values of $O_{47}$ (0.938558), $O_{48}$ (0.960604), $O_{49}$ (0.870570), $O_{51}$ (0.854430), $O_{54}$ (0.883411), $O_{56}$ (0.870113), $O_{58}$ (0.939208), $O_{59}$ (0.985411), $O_{61}$ (0.963891), $O_{62}$ (0.891047), $O_{64}$ (1.003079) and $O_{65}$ (0.855753) atoms were found to be highly negative values. This is because these atoms are largely electronegative. In addition, it is seen that $P_{46}$ (2.022931), $P_{53}$ (2.014757), and $P_{60}$ (1.983497) by HF method and atoms have higher Mulliken atomic charge than other positive atoms. The reason for this is that the neighboring atoms ($O_{47}$, $O_{48}$, $O_{49}$, $O_{51}$, $O_{54}$, $O_{56}$, $O_{58}$, $O_{59}$, $O_{61}$, $O_{62}$, $O_{64}$, and $O_{65}$) have significant electronegative properties.

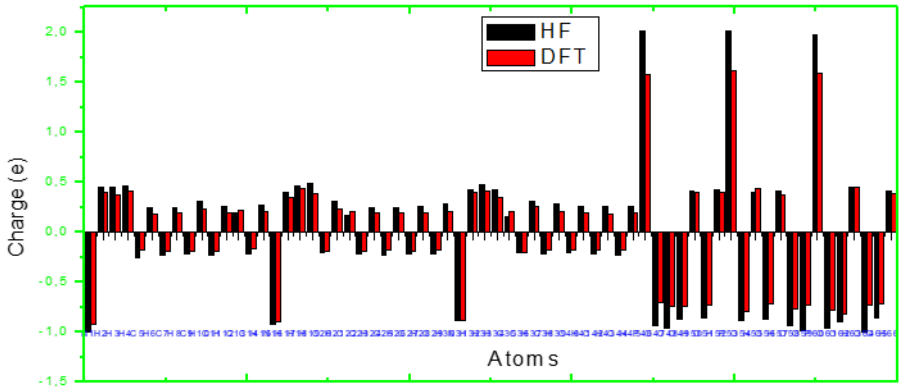


**Figure 12**. Mulliken charge distribution of ADHP compound.

## 4. Conclusions

In the present work, The fraction of intermolecular interactions of the title chemical is shown by the Hirshfeld surface analysis. Furthermore, the geometric properties of the inorganic entities are linked to one another by O-H...O hydrogen bonds, and both cations The components of anilinium and anions dihydrogen phosphate are bonded together by N-H...O and C-H...O hydrogen bonds, forming a three-dimensional network. The fraction of intermolecular contacts of the title chemical revealed by the Hirshfeld surface analysis shows that the H...O interactions are the most abundant (41.0%). Using the density functional theory (DFT/B3LYP) and Hartree-Fock methods with 3-21G basis sets, all of the theoretical computations were completed. The Study of the Mulliken Population and the Map of Molecular Electrostatic Potential (MEP) help each other to provide a better understanding of the chemically active regions. In fact, the result proves that there are good potential sites around atoms H. Electronegativity, chemical hardness, and softness have all been calculated. According to the measured tiny value, the compound under discussion is a hard system that is prone to chemical reactions. The energy between the HOMO and LUMO was also estimated (4.201 eV). We can infer that a molecule is hard if the HOMO-LUMO gap is wide. We can affirm that this material exhibits hybrid behavior and has an essential band gap energy of 4.201 eV based on the investigations into optical and luminescence activities.

## Funding

This research received no external funding.

## Acknowledgments

Declared none.

## Conflicts of Interest

Declare conflicts of interest.

## References

1. McNaughton, D. A.; Fares, M.; Picci, G.; Gale, P. A.; & Caltagirone, C. Advances in fluorescent and colorimetric sensors for anionic species. *Coordination Chemistry Reviews* **2021,** *427*, 213573, https://doi.org/10.1016/j.ccr.2020.213573.
2. Petersen, H.; Stegmann, N.; Fischer, M.; Zibrowius, B.; Radev, I.; Philippi, W.; & Weidenthaler, C. Crystal Structures of Two Titanium Phosphate-Based Proton Conductors: Ab Initio Structure Solution and Materials Properties. *Inorganic Chemistry* **2022,** *61***,** 2379–2390, https://doi.org/10.1021/acs.inorgchem.1c02613.
3. Rafik, A.; Zouihri, H.; Guedira, T.; ONE-DIMENSIONAL HYDROGEN-BONDED N–H…O IN THE HYBRID PHOSPHATE: HIRSHFELD SURFACE ANALYSIS AND DFT QUANTUM CHEMICAL CALCULATIONS, *Chem. Chem. Technol* **2021,** *15*, 3,359–368, https://doi.org/10.23939/chcht15.03.359.
4. Xu, Y. L.; Cai, Y.; Yu, J. Y.; Xu, Y.; Yang, Y.; Fang, S. H.; ... & Ni, C. L. Syntheses, crystal structures, antibacterial activities and nonlinear optical properties based on DFT calculation of two substituted benzyl piperidinium salts tetrahalogenated copper (II). *Journal of Molecular Structure*, **2022,** *1256*, 132543, https://doi.org/10.1016/j.molstruc.2022.132543.
5. Sonia, N. ; Vijayan, V. ; Mahak, K. ; Anuj, Y. ; Harsh, K. K. ; Maurya, S. A.; Britto Dhas, M. ; Prashant. K. An efficient piezoelectric single-crystal l-argininium phosphite: structural, Hirshfeld, electrical and mechanical analyses for NLO applications. *J. Applied Physics A,* **2019,** *125*, 363–377, https://doi.org/10.1007/s00339-019-2642-5.
6. Bai, C.; Wei, F. H.; Hu, H. M.; Yan, L.; Wang, X.; & Xue, G. L. New highly luminescent europium (III) complex covalently bonded with titania-based host via using a terpyridine carboxylate derivative linker for fluorescence sensing. *Journal of Luminescence* **2020,** *227*, 117545-117555, https://doi.org/10.1016/j.jlumin.2020.117545.
7. Kessentini, Y.; Ahmed, A. B.; Al-Juaid, S. S.; Elaoud, Z. Phase transition, nonlinear optical parameters and electrical properties in 4-benzylpiperidinium tetraoxoselenate monohydrate. *Journal of Solid State Chemistry* **2022**, 313,123286, https://doi.org/10.1016/j.jssc.2022.123286.
8. Rafik, A.; Zouihri, H.; Guedira, T. HIRSHFELD SURFACE ANALYSIS AND QUANTUM CHEMICALSTUDY OF MOLECULAR STRUCTURE OF PHOSPHATE. *Bull. Chem. Soc. Ethiop.* **2021,** *35*, 625-638. https://dx.doi.org/10.4314/bcse.v35i3.13.
9. Feriel, H.; Arfaoui, Y.; Silvestru, C.; & Bourguiba, N. F. Synthesis, structural and spectroscopic studies, DFT calculations, thermal characterization and Hirshfeld surface analysis of copper (II) organic-inorganic hybrid material $(C_{12}H_{22}N_2)[CuCl_4]$. *Journal of Coordination Chemistry* **2022,** 1-14, https://doi.org/10.1080/00958972.2022.2039642.
10. Barhoumi, A.; Mahroug, A.; Josep Suñol, J.; Belhouchet, M. Synthesis, crystal structure, Hirshfeld surface analysis and DFT calculations of a new benzidinium phosphate, *Inorganic Chemistry Communications* **2021,** *133*, 108905-108915, https://doi.org/10.1016/j.inoche.2021.108905.
11. Fellahi, Z.; Hannachi, D.; Djedouani, A.; Ouksel, L.; François, M.; Fleutot, S.; & Bourzami, R. Synthesis, X-ray crystallography, Hirshfeld surface analysis, thermal properties and DFT/TD-DFT calculations of a new material hybrid ionic $(C_{10}H_{18}N_2O_8^{2+}.\ 2ClO_4^{-}.\ 4H_2O)$. *Journal of Molecular Structure* **2021,** *1244*, 130955-130970, https://doi.org/10.1016/j.molstruc.2021.130955.
12. Frisch, M. J.; Trucks, G.W.Y. ; Schlegel, H. B. ; Scuseria, G. E.; Robb, M. A.; Cheeseman, J. R. ; Montgomery, J. A. ; Vreven, J. ; Kudin, T.; Burant, K.N. ; Millam, J. C. ; Iyengar, J. M. ; Tomasi, S.S.; Barone, J. ; Mennucci, V. ; Cossi, B.; Scalmani, M.; Rega, G. ; Petersson, N.; Nakatsuji, G. A. ; Hada, H. ; Ehara, M.; Toyota, M.; Fukuda, K. ; Hasegawa, R. ; Ishida, J.; Nakajima, M.; Honda, T.; Kitao, Y. ; Nakai, O.; Klene, H.; Li, M.; Knox, X. ; Hratchian, J. E.; Cross, H. P. ; Adamo, J. B.; Jaramillo, C.; Gomperts, J.; Stratmann, R.; Yazyev, R.E.; Austin, O.; Cammi, A.J.; Pomelli, R.; Ochterski, C. ; Ayala, J.W.; Morokuma, P.Y.; Voth, K.; Salvador, G. A.; Dannenberg, P.; Zakrzewski, J. J.; Dapprich, V.G.;

Daniels, S. ; Strain, A. D. ; Farkas, M. C.; Malick, O.; Rabuck, D. K. ; Raghavachari, A.D. ; Foresman, K.; Ortiz, J. B. ; Cui, J. V. ; Baboul, Q.; Clifford, A. G. ; Cioslowski, S. ; Stefanov, J.; Liu, B. B.; Liashenko, G.; Piskorz, A.; Komaromi, P.; Martin, I. ; Fox, R. L.; Keih, D. J.; Al-Laham, T.; Peng, M.A.; Nanayakkara, C. Y.; Challacombe, A. ; Gill, M.; Johnson, P. M. W.; Chen, B. ; Wong, W. ; Gonzalez, M. W. ; Pople, C. Gaussian 03, Gaussian Inc., Pittsburg, PA, **2003**, https://gaussian.com/citation_a03/.

13. Labanowski, J. K.; Andzelm. J.W. Density Functional Methods in Chemistry. New York: *Springer Verlag* **1991,** https://link.springer.com/book/10.1007/978-1-4612-3136-3.
14. Lee, C.; Yang, W.; Parr, R. G. Development of the Colle-Salvetti correlation-energy formula into a functional of the electron density. *Phys Rev B.* **1988,** *37*, 785-789, https://doi.org/10.1103/PhysRevB.37.785.
15. Frish, A.; Nielsen, A.B.; Holder, A.J. GAUSSVIEW User Manual, Gaussian Inc., Pittsburg, PA. **2001,** http://wild.life.nctu.edu.tw/~jsyu/compchem/g09/g09ur/m_citation.htm.
16. Spackman, P. R.; Turner, M. J.; McKinnon, J. J.; Wolff, S. K.; Grimwood, D. J.; Jayatilaka, D. & Spackman, M. A. *J. Appl. Cryst.* **2021,** *54*, 1006–1011, https://doi.org/10.1107/S1600576721002910.
17. Spackman, M.A.; Byrom, P.G. A novel definition of a molecule in a crystal. *Chem. Phys. Lett*. **1997,** *267*, 215-220, https://doi.org/10.1016/S0009-2614(97)00100-0.
18. Parkin, A.; Barr, G.; Dong, W.; Gilmore, C.J.; Jayatilaka, D.;McKinnon, J.J.; Spackman, M.A. ; Wilson. C.C. Comparing entire crystal structures: structural genetic fingerprinting, *CrystEngComm* **2007,** *9*, 648-652, https://doi.org/10.1039/B704177B.
19. Spackman, M.A.; Jayatilaka. D. Hirshfeld surface analysis. *CrystEngComm* **2009**, *11*, 19-32, https://doi.org/10.1039/B818330A.
20. Jelsch, C.; Ejsmont, K.; Huder, L. The enrichment ratio of atomic contacts in crystals, an indicator derived from the Hirshfeld surface analysis. *IUCrJ* **2014,** *1*, 119-128, https://doi.org/10.1107/S2052252514003327.
21. Matta, C.F.; Hern andez-Trujillo, J.; Tang, T.H.; Bader, R.F.W. Hydrogen–Hydrogen Bonding: A Stabilizing Interaction in Molecules and Crystals. *Chem. Eur. J.* **2003,** *9*, 1940-1951, https://doi.org/10.1002/chem.200204626.
22. Turner, M. J. ; MacKinnon, J. J.; Wolff, S. K.; Grimwood, D. J.; Spackman P. R.; Jayatilaka, D.; & Spackman A M . *CrystalExplorer17.5*. University of Western Australia **2017,** *4*, 575–587, https://doi.org/10.1107/S205225251700848X.
23. 23. Yaman, M.; Almarhoon, Z. M. ; Cakmak, S. ; Ku¨tu¨ k, H. ; Meral, G. ; & Dege, N. Crystal structure of 2, 3-dimethoxy-N-(4-nitrophenyl) benzamide. *Acta Cryst*, **2018,** *74*, 41–44, https://doi.org/10.1107/S2056989017017741.
24. 24. Turner, M. J.; McKinnon, J. J.; Jayatilaka D.; and Spackman, M. a. Visualisation and characterisation of voids in crystalline materials. *CrystEngComm* **2011,** *13***,** 1804-2011, https://doi.org/10.1039/C0CE00683A.
25. 25. Ashfaq, M.; Tahir, M. N.; Kuznetsov, A.; Mirza, S. H.; Khalid, M.; & Ali, A. DFT and single crystal analysis of the pyrimethamine-based novel co-crystal salt: 2, 4-diamino-5-(4-chloro-phenyl)-6-ethylpyrimidin-1-ium: 4-hydroxybenzoate: methanol: hydrate (1: 1: 1: 1)(DEHMH). *Journal of Molecular Structure* **2020,** *1199*, 127041-127051, https://doi.org/10.1016/j.molstruc.2019.127041.
26. Kanagathara, N.; MaryanjalIn, F.; Ragavendran, V.; et al. Experimental and theoretical (DFT) investigation of crystallographic, spectroscopic and Hirshfeld surface analysis of anilinium arsenate. *Journal of Molecular Structure* **2021,** *1223*, 128965-128980 https://doi.org/10.1016/j.molstruc.2020.128965.
27. Dubey, R.P.; Patel, Urmila H.; Pandya, S. B Chaudhary, K. P.; Socha, B. N. Cadmium complex of sulfathiazole dihydrate with secondary ligand pyridine: structure, DFT studies, Hirshfeld surface analysis and antimicrobial activity. *Indian Journal of Physics* **2021,** *95*, 33-42, https://doi.org/10.1007/s12648-019-01680-8.
28. Gadre, S. R.; Suresh, C. H.; Mohan, N. Electrostatic potential topology for probing molecular structure, bonding and reactivity. *Molecules* **2021,** *26*, 3289, https://doi.org/10.3390/molecules26113289
29. Fleming I. Frontier Orbitals and Organic Chemical Reactions. *First ed., Wiley, London, UK* **1976,** https://www.abebooks.co.uk/9780471018193/Frontier-Orbitals-Organic-Chemical-Reactions-0471018198/plp
30. Karrouchi, K.; Fettach, S.; Jotani, M.M.; Sagaama, A.; Radi, S.; Ghabbour, H. A.; Mabkhot, Y.N.; Himmi, B.; Faouzi, M.A.; Issaoui, N. analysis, DFT calculations, anti-diabetic activity and molecular docking studies of (E)-N'-(5-bromo-2-hydroxybenzylidene) isonicotinohydrazide, *Journal of Molecular Structure* **2020,** *1221*, 128800-128846, https://doi.org/10.1016/j.molstruc.2020.128800.
31. Noureddine, O.; Gatfaoui S.; Brandan, S. A.; Sagaama, A.; Marouani, H.; Issaoui, N. Experimental and DFT studies on the molecular structure, spectroscopic properties, and molecular docking of 4-

phenylpiperazine-1-ium dihydrogen phosphate, Journal of Molecular Structure **2020,** *1207*, 127762- 127778, https://doi.org/10.1016/j.molstruc.2020.127762.

32. Hussain, I; Hussain, T.; Ahme, S.B.; Thanayut, K.; Muhammad, A.; Xi, C.; Muhammad, S. J.; Charmaine, L.; Kaili Z. Binder-free trimetallic phosphate nanosheets as an electrode: Theoretical and experimental investigation. *Journal of Power Sources* **2021**,513, 230556,https://doi.org/10.1016/j.jpowsour.2021.230556.
33. Marahatta, A. B. Computational study on electronic structure, atomic charges distribution and frontier molecular orbitals of butadiene: general features for diels-alder reaction. *International Journal of Progressive Sciences and Technologies* **2020,** *19*, 48-64. http://dx.doi.org/10.52155/ijpsat.v19.2.1648.
34. Medimagh, M.; Issaoui, N.; Gatfaoui, S.; Al-Dossary, O.; Kazachenko, A. S.; Marouani, H.; & Wojcik, M. J. Molecular modeling and biological activity analysis of new organic-inorganic hybrid: 2-(3, 4-dihydroxyphenyl) ethanaminium nitrate. *Journal of King Saud University-Science* **2021,** 33, 101616. https://doi.org/10.1016/j.jksus.2021.101616.
35. Adole, V. A.; Koli, P. B.; Shinde, R. A.; & Shinde, R. S. Computational insights on molecular structure, electronic properties, and chemical reactivity of (E)-3-(4-chlorophenyl)-1-(2-hydroxyphenyl) prop-2-en-1-one. *Material Science Research India* **2020,** *17*, 41-53, http://dx.doi.org/10.13005/msri.17.special-issue1.06.